Ceramics International 45 (2019) 160–167

Contents lists available at ScienceDirect

Ceramics International

journal homepage: www.elsevier.com/locate/ceramint

Electrochemical effect of graphite fluoride modification on Li-rich cathode material in lithium ion battery

Bing Jiang[1], Bi Luo[1], Jingru Li, Peng Peng, Jiewei Chen, Lihua Chu, Yingfeng Li, Meicheng Li*

State Key Laboratory of Alternate Electrical Power System with Renewable Energy Sources, School of Renewable Energy, North China Electric Power University, Beijing 102206, China

ARTICLE INFO

Keywords:
Li-rich layered cathodes
Surface modification
Lithium-ion battery
Graphite fluoride

ABSTRACT

Recently, Li-rich layered structure has been used in the cathode of lithium ion batteries because of its high specific capacity. However, this structure still has some problems including large irreversible capacity loss, significant deterioration of cycling performance and poor rate property. Therefore, in our study, graphite fluoride is used to modify the surface of $Li_{1.14}Ni_{0.133}Co_{0.133}Mn_{0.544}O_2$ through a facile solvent evaporating method. Due to conversion reaction of the graphite fluoride, the huge discharge capacity compensation during the first discharging can improve the coulombic efficiency significantly. As reaction products, the layer of LiF@carbon reduces the interfacial reactions and increases the reversible capacity. After modification by graphite fluoride, the discharge capacities are improved by 22% from 266 to 325 mAh g^{-1} at 0.1 C, and 13% at 2 C. After 100 cycles, the discharge capability at 1 C is increased by 13% from 180 to 203 mAh g^{-1}.

1. Introduction

With the wide applications in the large-scale energy storage devices and electronics, more researches focus on the high capacity, larger energy density and more cycles of Li-ion battery [1–7]. The conventional cathode materials, like layer structural $LiCoO_2$, spinel structural $LiMn_2O_4$ and olive structural $LiFePO_4$ cannot meet the above requirement satisfactorily. Recently, Li-rich layer structural oxides ($xLi_2MnO_3 \cdot (1-x)LiMO_2$ ($0 < x < 1$, M = Ni, Co, Mn)) have the higher specific capacity and larger energy density, which have attracted more interests of researchers [8–10]. However, this layered oxide is restricted in practical commercial applications due to its large capacity loss during the first charging, rapid capacity degradation and poor rate property. [11,12]. The capacity loss during the first charging is proposed to be ascribed to the electrochemical activation of the Li_2MnO_3 with the releasing of the oxygen and lithium ion (when charged above 4.4 V), which results in a low coulombic efficiency in the first discharging [13].

Many studies focus on the modification strategies, which can enhance the electrochemical property of this kind layer structural oxide. Researchers found that coating layers of metallic oxide [14,15], fluoride [16,17], phosphate [18,19] could increase the electrochemical properties by decreasing the reactions in the interface between electrolyte and cathode and reducing the cathode dissolution. Zhao [16] designed a protective layer of LiF/FeF_3 outside $Li[Li_{0.2}Ni_{0.2}Mn_{0.6}]O_2$, in which LiF could suppress interfacial side reactions and conversion reaction effectively. Zhuo [20] modified $Li[Li_{0.1}Ni_{0.45}Mn_{0.45}]O_2$ by the carbon similar to graphene, which could suppress interfacial side reactions and decrease the manganese dissolution. Therefore, the LiF and carbon are effective coating layer components for Li-rich cathodes. As a cost-effective and industrialized cathode, graphite fluoride ($(CF_x)_n$) has been used for primary batteries for many years [21–23]. Graphite fluoride can deliver a large irreversible capacity with the productions of LiF and carbon during the first discharging. Due to the actions of LiF and carbon, graphite fluoride ($(CF_x)_n$ is a probable modified material for the Li-rich oxides, which may improve initial coulombic efficiency and discharge capacity.

In this study, graphite fluoride ($(CF_x)_n$, $x = 1$) is used to modify the surface of $Li_{1.14}Ni_{0.133}Co_{0.133}Mn_{0.544}O_2$ (LRNCM) through a facile mild and solvent evaporating method to improve the electrochemical property, especially the initial coulombic efficiency. The cycle performance and rate property of LRNCM cathode batteries are analyzed in the 2.0–4.8 V range.

2. Experimental details

2.1. Materials preparation

The carbonate coprecipitation method was used to prepare

* Corresponding author.
E-mail address: mcli@ncepu.edu.cn (M. Li).
[1] These authors contribute equally to this work.

https://doi.org/10.1016/j.ceramint.2018.09.147
Received 20 August 2018; Received in revised form 11 September 2018; Accepted 13 September 2018
Available online 20 September 2018

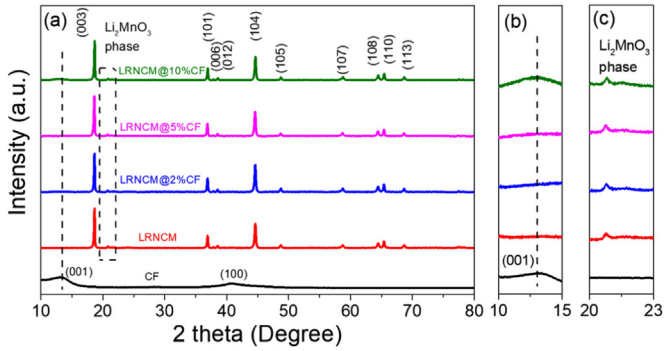

Fig. 1. X-ray diffraction data of pristine LRNCM, LRNCM@CF and pure CF specimens.

$Li_{1.14}Ni_{0.133}Co_{0.133}Mn_{0.544}O_2$. Stoichiometric amount of $CoSO_4{\cdot}7H_2O$, $MnSO_4{\cdot}4H_2O$ and $NiSO_4{\cdot}6H_2O$ were dissolved into deionized water, which is titrated into Li_2CO_3 solution. The resulting coprecipitated carbonates powders were washed by distilled water, and then dried in a vacuum environment at 80 °C for over 20 h. After that, the powders were mixed with Li_2CO_3 which has the corresponding stoichiometric to above coprecipitation process. The mixed powders were ground for 30 min, and then pre-treated at 500 °C for 5 h and a followed calcination of 850 °C for 15 h in the air.

The different mass ratios of $(CF)_n$ powders were ultrasonic dispersed in ethyl alcohol for 120 min. $Li_{1.14}Ni_{0.133}Co_{0.133}Mn_{0.544}O_2$ powder was mixed with $(CF)_n$ solution by a magnetic stirring at 55 °C for 30 min and dried at 120 °C for 10 h. Finally, the obtained samples are denoted here below as LRNCM@2%CF, LRNCM@5%CF, LRNCM@10%CF.

2.2. Characterization

The morphology of the cathode materials was investigated by Scanning Electron Microscope (SEM, Hitachi SU8010) and Transmission Electron Microscope (TEM, Tecnai G2 F20). The crystalline structure of cathode materials was assessed with X-ray diffraction (XRD, BRUKER, D8 Focus, Germany) using the Cu-Ka radiation with 10–80° incidence angle. X-ray Photoelectron Spectroscopy (XPS, ESCALAB 250Xi) were used to investigate the surface of the cathode materials. All XPS spectra were corrected by using the C 1s (C–C, C–H) signal at 284.6 eV [24].

2.3. Electrochemical measurements

To prepare cathode electrode, the slurry consisting of 90 wt% pristine or CF-modified, 5 wt% acetylene black (Super-P) and 5 wt% polyvinylidene fluoride (PVDF) was spread on the aluminum foil and then vacuum dried at 110 °C for 14 h. CR2032-type coin half-cell was assembled in Ar-filled glove box (H_2O and O_2 0.1 < ppm). The device is composed by the cathode electrode (Li-rich materials), anode (Li metal), separator (glass fiber, Whatman), and electrolyte (1 M $LiPF_6$/EC-DMC). The cell was galvanostatically charged and discharged between 2.0 and 4.8 V vs Li/Li^+ (1 C is 200 mAg^{-1}) using a multichannel battery test system (Land, China). An electrochemical impedance spectrum (EIS) was recorded with the electrochemical workstation (Zahner Zennium) under 10 mV and a 100 kHz to 0.01 Hz range.

3. Results and discussion

3.1. Cathode materials characterizations

Fig. 1 shows the structural information of pristine LRNCM and LRNCM@CF by XRD measurements. The main diffraction peaks of pristine LRNCM and LRNCM@CF samples are well indexed to a typical α-$NaFeO_2$ structure, except some superstructure peaks between 20° and 25° [5,25–27]. Highly ordered layered structure of pristine LRNCM and LRNCM@CF samples are reflected by these obvious peaks and peak

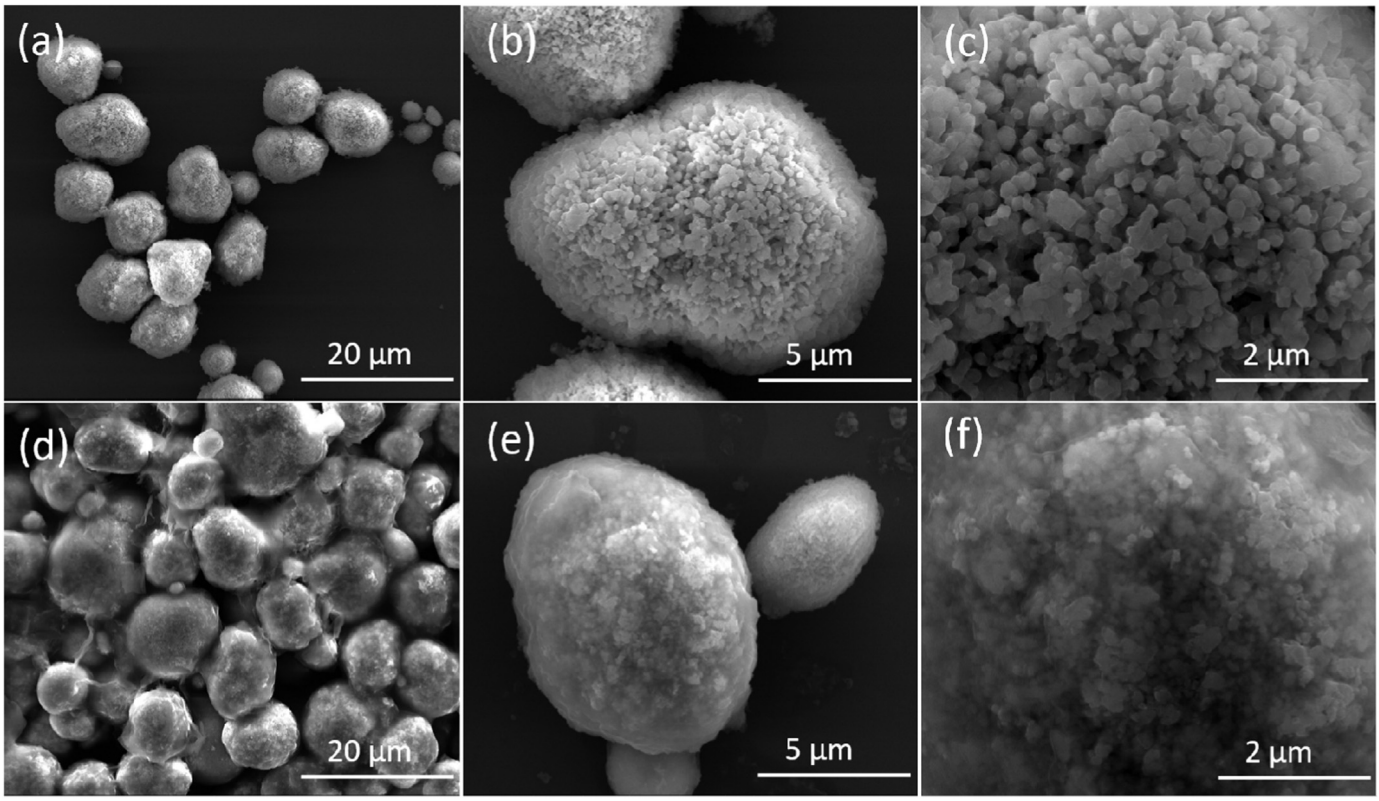

Fig. 2. SEM morphology of (a-c) pristine LRNCM particles and (d-f) LRNCM @2%CF particles under different magnification.

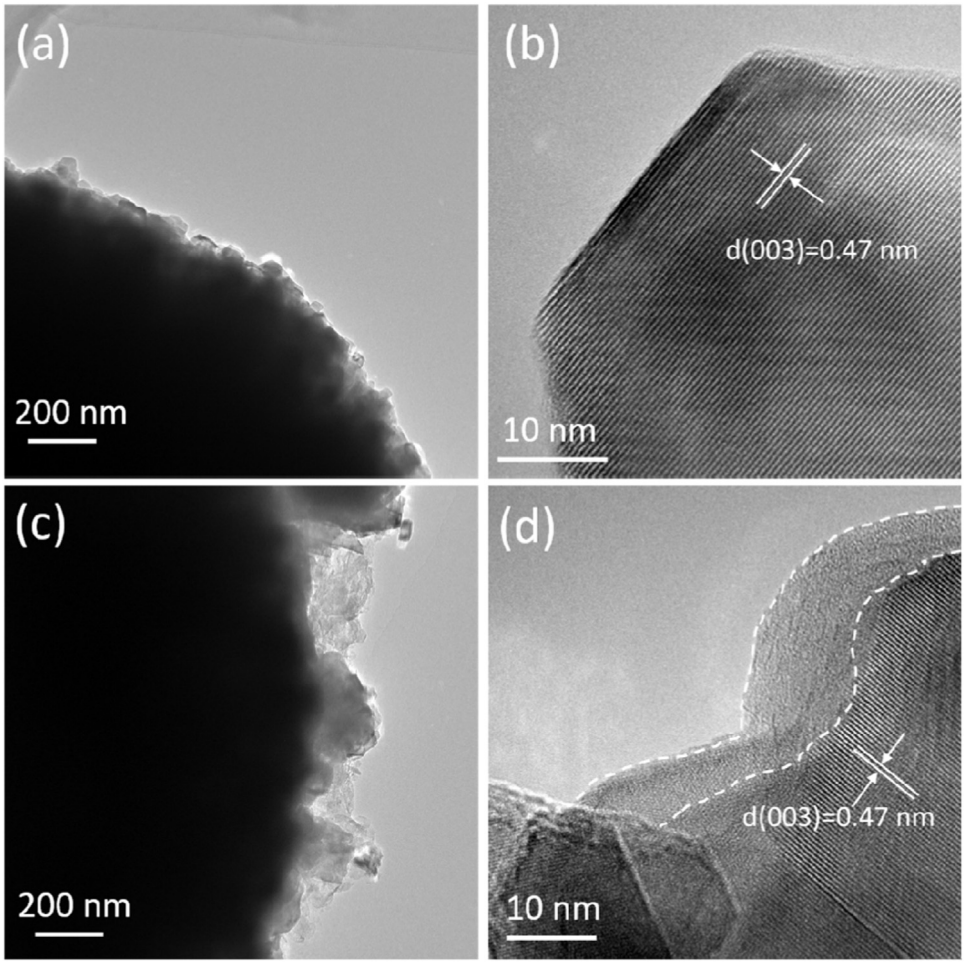

Fig. 3. TEM and HR-TEM images of (a-b) pristine LRNCM particle and (c-d) LRNCM@5%CF particle.

splits of (006)/(102) and (018)/(110) [28,29]. The small peaks between 20° and 25° are the diffractions of Li^+ and Mn^{4+} in Li_2MnO_3 structure (C2/m) [16,17]. In the diffraction of LRNCM@10%CF samples, the wide-ranged peaks between 10° and 15° are corresponding to the (001) diffraction of pure CF specimens. The (001) and (100) diffractions of pure CF specimens are consistent with the typical position for graphite fluoride reported in prior studies [30,31]. Therefore, the crystalline structure of LRNCM@CF is not changed obviously by modification, which indicates that the CF coating is a mild process.

The surface morphology and particle sizes of pristine LRNCM and LRNCM@CF samples are shown in Fig. 2 and Fig. S1. The results show that pristine LRNCM and LRNCM@2%CF secondary spherical particles have a similar size of about 5–10 μm. Compared with pristine LRNCM, an obvious film is observed on the particle surface after modification. With the mass ratios of (CF)n powders increasing to 20%, some superfluous CF slices are observed due to the stronger binding force between CF and CF, which can affect the formation of CF film on the surface of LRNCM. Furthermore, TEM images of the pristine LRNCM and LRNCM@CF samples are shown in Fig. 3 and Fig. S2. The higher mass ratios of (CF)n powders can contribute to a thicker coating layer. The measured inter-planar distance is 0.47 nm in the crystallized areas, which matches well to the (003) crystal planes of LRNCM. From Fig. 3(d), a coating layer about 10 nm thicknesses was observed on the surface of LRNCM.

XPS were used to analyze the composition and chemical states of pristine LRNCM and LRNCM @5%CF samples. From Fig. 4(a) and (b), the F 1s peak at 688.57 eV can be seen obviously in the LRNCM @5%CF samples, which is corresponding to the semi-ionic C-F bond of graphite fluoride [22,32], whereas there is no peak of F 1s in the pristine LRNCM samples. It can be seen from Fig. 4(c) that there is an obvious change in C 1s spectra, which comes from C element in coating layer of LRNCM @ 5%CF samples. It is found that the main peak shifts from 289.8 eV to 284.8 eV after CF modification. The peaks at 289.8 and 291.7 eV in LRNCM @5%CF samples are corresponding to $F\underline{C}(C)_3$ and $F\underline{C}(CF)_3$ moieties, which are associated with the bonding and the distributions of F in the carbon matrix [22].

The high-resolution XPS spectra of Ni 2p, Co 2p, and Mn 2p are shown in Fig. 4(d) and Fig. S3, which indicate that the valence states of Ni, Co and Mn of LRNCM and LRNCM @5%CF samples are corresponding to 2 +, 3 + and 4 +, respectively [33,34]. Moreover, the ratios of satellite peaks in Ni 2p spectra for the LRNCM @5%CF samples surface have an increase in Fig. 4(d). To investigate the reason for this change of Ni element, the XPS spectra of pure CF sample is also shown in Fig. S4. It is found that the Ni 2p peaks exists in the spectra of pure CF sample, which comes from the Ni impurities during the synthesis process of graphite fluoride. In addition, the depth profile of Ni 2p is revealed by XPS with ion sputtering for 30 s, 60 s and 90 s, as shown in Fig. 4(e) and (f). The Ni 2p peaks in Fig. 4(f) just has a little difference between before and after ion sputtering (black line), whereas after sputtering 30 s the binding energy of Ni 2p peaks have a similar spectra (red, line and pink lines). The results indicate that CF layer can be coated on the surface of LRNCM and has no effect on the bulk phase of LRNCM.

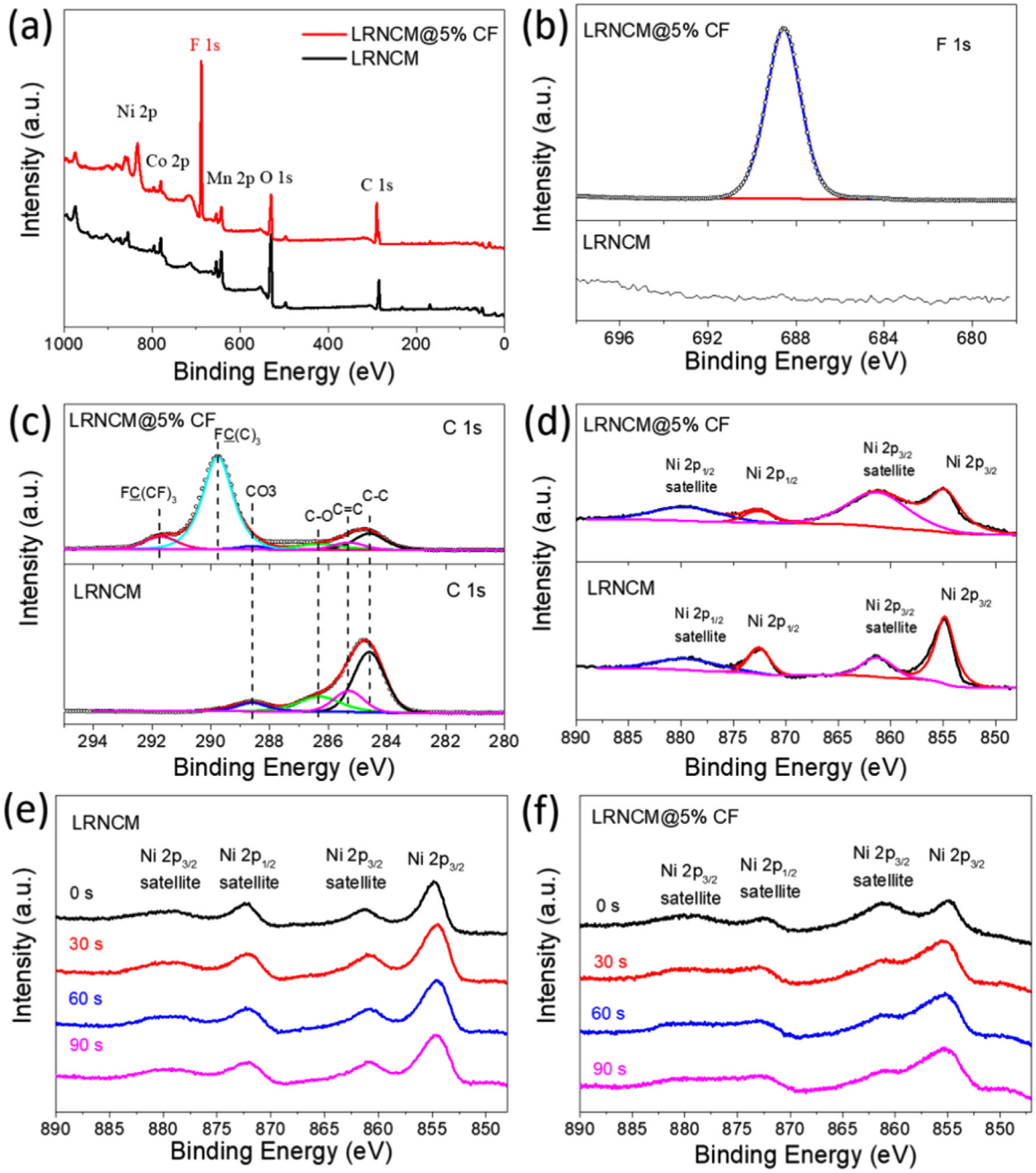

Fig. 4. XPS spectra of pristine LRNCM and LRNCM@5%CF samples: (a) XPS survey spectra; (b) F 1 s;(c) C 1 s; (d) Ni 2p; (e-f) the depth profile of Ni 2p.

3.2. Electrochemical performance

The electrochemical performance of cells were investigated by galvanostatic charge-discharge experiments between 2.0 and 4.8 V. Fig. 5(a) and (b) compares the charge-discharge curves of the beginning two cycles of pristine LRNCM and LRNCM@CF samples. Obviously, the additional discharging plateau of LRNCM@CF samples is at 2.4 V during the first cycle, which is ascribed to the conversion reaction of (CF)n to LiF. This electrochemical process is described by the following equation [35,36]:

$$CFx + xLi^{+} + xe^{-} \rightarrow C + xLiF \quad (1)$$

However, no corresponding charging plateau around 2.4 V exists in the 2nd charging process and no similar discharging plateau appears in the 2nd discharging process, indicating that the transformation process of LiF is irreversible. According to the equation, as the reaction products LiF@carbon coating layer can generate on the surface of LRNCM after initial discharging. In Fig. 5(a), the initial charge and discharge capacities of the pristine LRNCM samples are 367 and 284 mAh g^{-1}, respectively, with the 77% coulombic efficiency. From the data of Table 1, the LRNCM@CF samples have the higher capacity and initial coulombic efficiency. For LRNCM@10%CF samples, the charge and discharge capacity are 392 and 390 mAh g^{-1}, respectively. Meanwhile the coulombic efficiency is significantly improved to 99%. Moreover, Fig. 5(c)-(f) shows the differential capacity versus voltage (dQ/dV) curves, in which the oxidation peak around 3.9 V is ascribed to the reversible Ni^{2+}/Ni^{4+} oxidation process [18,37]. The oxidation peak around 4.4 V in the first cycle is related to the partially reversible anionic O^{2-}/O^{2-x} and irreversible loss of oxygen in first charging [11,37], accompanied by an irreversible capacity loss. The reduction peak around 2.4 V in the first cycle is attributed to the irreversible reaction of CF. Therefore, in our studies, the CF coating layer

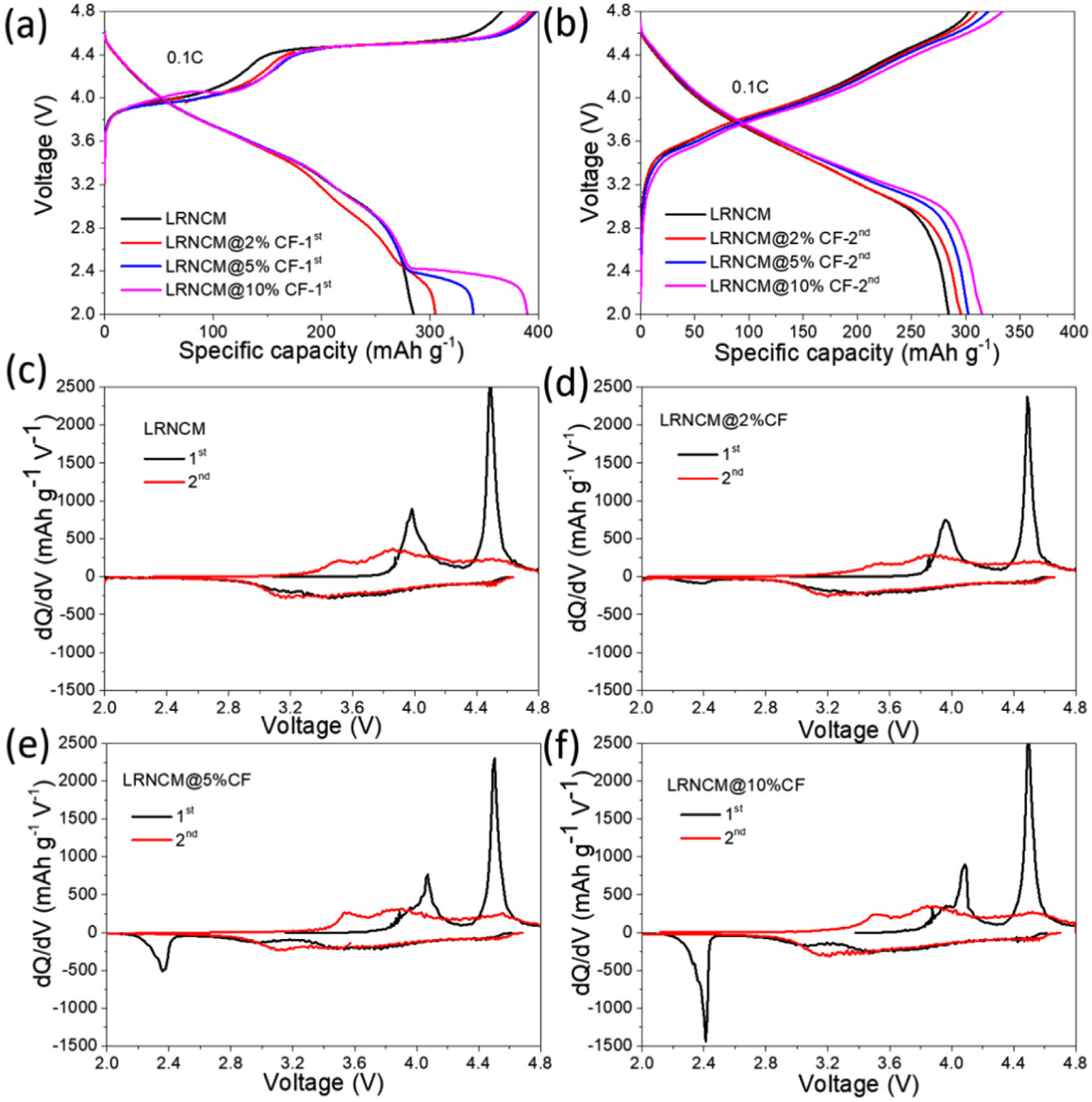

Fig. 5. Charge–discharge characteristics of pristine LRNCM and LRNCM @CF sample: the (a) first and (b) second cycle curves; (c-f) the corresponding differential capacity versus voltage (dQ/dV) curves.

Table 1
Comparison of the initial capacity and coulombic efficiency for the pristine LRNCM and LRNCM@CF samples at 0.1 C.

Samples	The 1st charge capacity (mAh g^{-1})	The 1st discharge capacity(mAh g^{-1})	Initial coulombic efficiency(%)
LRNCM	369	281	76
LRNCM@ 2%CF	396	305	77
LRNCM@ 5%CF	398	340	85.4
LRNCM@ 10%CF	392	390	99.5

compensates the capacity loss of LRNCM and significantly increase the coulombic efficiencies in the first cycle.

The cycling performance of pristine LRNCM and LRNCM@CF samples at 0.1 C and 1 C are shown in Fig. S5 and Fig. 6(a), respectively. From Fig. S5, the LRNCM sample shows a discharged capacity at 240.2 mAh g^{-1} after 30 cycles at 0.1 C. After modification, the discharge capacity of LRNCM@ (2%, 5%, 10%) CF samples increase to 250.6, 266.6 and 273.5 mAh g^{-1}, respectively. For Fig. 6(a), the first two cycles were activated under 0.1 C, and the following cycles were performed under 1 C. The discharge capacity after 100 cycles for the pristine LRNCM is 180 mAh g^{-1}, which is similar to the values previously reported [16,38]. After modification, the discharge capacity of LRNCM@(2%, 5%, 10%) CF samples increase to 184, 196 and 203 mAh g^{-1} (by 2%, 9% and 13%), respectively. In Fig. 6(b), the LRNCM@CF samples have more discharge capacity below 3.5 V regions compared with the pristine LRNCM. Therefore, the discharge capacities are plotted into two regions that below and above 3.5 V vs Li/Li^+. The results show that the discharge capacity of LRNCM@CF samples at the high-potential region is similar to that of pristine LRNCM (> 3.5 V vs Li/Li^+), whereas, the capacity of LRNCM@CF is obviously improved in the region below 3.5 V. From SEM images (Fig. S6) of the LRNCM@CF and the pristine LRNCM after cycles, the pristine LRNCM after cycles are rough due to the damage during cycling, while LRNCM@CF can be preserved well. The LiF@carbon coating layer on the surface of particles, acting as a protective layer, which can decrease the direct contact between the electrolyte and electrode. Therefore, the layer can suppress

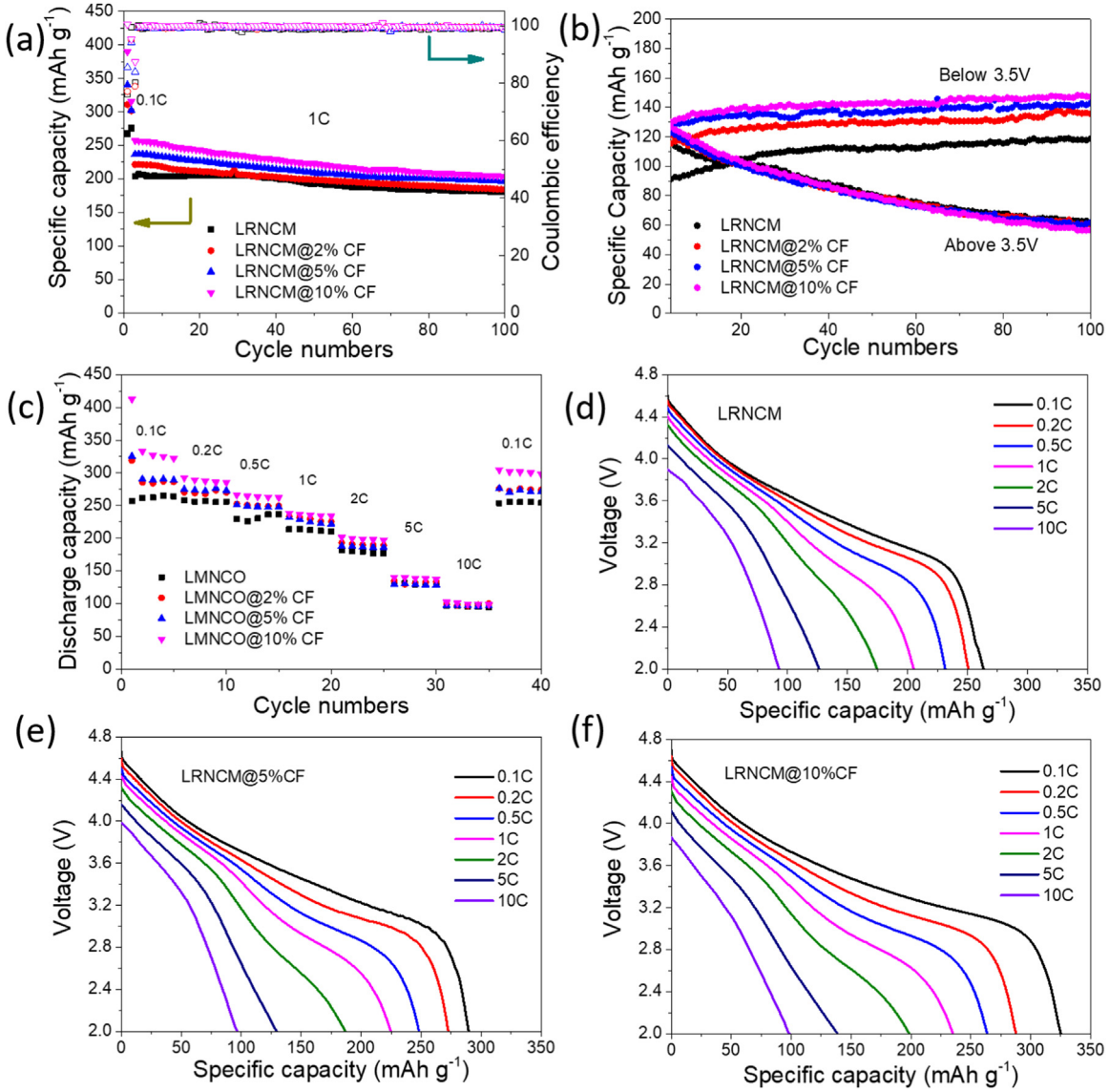

Fig. 6. The electrochemical property of pristine LRNCM and LRNCM @CF samples: (a) The cycling performance; (b) discharge capacity above and below 3.5 V vs Li/Li^+ during cycling at 1 C; (c) the rate performance; (d-f) the discharge curve at different rates.

interfacial side reactions and dissolution of transition metal elements during cycling resulting in the significant improvement of the reversible capacity.

The rate capability of pristine LRNCM and LRNCM@CF samples with different proportions CF under 0.1 C, 0.2 C, 0.5 C, 1 C, 2 C, 5 C and 10 C, as shown in Fig. 6(c). With increasing current rate, the specific capacities of all samples reduce due to the electrochemical polarization. Fig. 6(c) shows that the LRNCM@10%CF samples exhibit a higher rate capability below 2 C. The discharge capacities of the pristine LRNCM samples are about 266, 255, 230, 210, 177, 131 and 95 mAh g^{-1} corresponding to the different current rate, respectively. The discharge capacities of LRNCM@10%CF samples are about 325, 288, 265, 237, 200, 140 and 100 mAh g^{-1}. With the cycling and current density increasing, the interfacial reactions between LRNCM and electrolyte can be aggravated, resulting in the increase of charge transfer resistance. Therefore, the restraint of the Li-ion transport between the cathode and the electrolyte is an another important reason for the poor rate capability of the pristine LRNCM. For the CF-modified LRNCM, the higher mass ratios of (CF)n samples can generate a thicker and more uniform LiF@carbon coating layer, which more effectively protect the LRNCM and reduce the increase of charge transfer resistance. Meanwhile, with the LiF@carbon layer thickening, the increase of C and LiF improve electrical conductivity and ionic conductivity on the surface, which can effectively improve the lithium ion diffusion and reduce the impedance of the batteries. In consequence, the LRNCM@CF samples deliver the improved rate capability below 2 C rate. However, at high rate (5 C and 10 C) the performance has no strong correlation with the electronic conductivity, and is limited mainly by the lithium ion diffusion in the bulk LRNCM layered structure [12,39]. The LiF@carbon coating layer can facilitate the electrical conductivity and ionic conductivity of the surface of LRNCM, but can't change the lithium ion diffusion in bulk matarials. Therefore, there is no obvious improvement at larger current densities (5 C and 10 C) for the LRNCM@CF samples.

The EIS measurements are conducted to investigate the electrochemical resistance after charging to 4.8 V. Fig. 7(a) and (b) show Nyquist plots of the LRNCM and LRNCM@10%CF cathodes after different cycles. The plots at an enlarged scale are shown in the insets. The EIS plots of each electrode consist of resistances of solution resistance (R_{sol}), resistances of surface film (R_{sf}), resistances of charge transfer (R_{ct}), and Warburg impedance (Z_w), respectively [4,40–44]. Fig. 7(c) is the corresponding equivalent circuit model. The resistance values are calculated by the equivalent circuit model, as shown in Table 2. On one

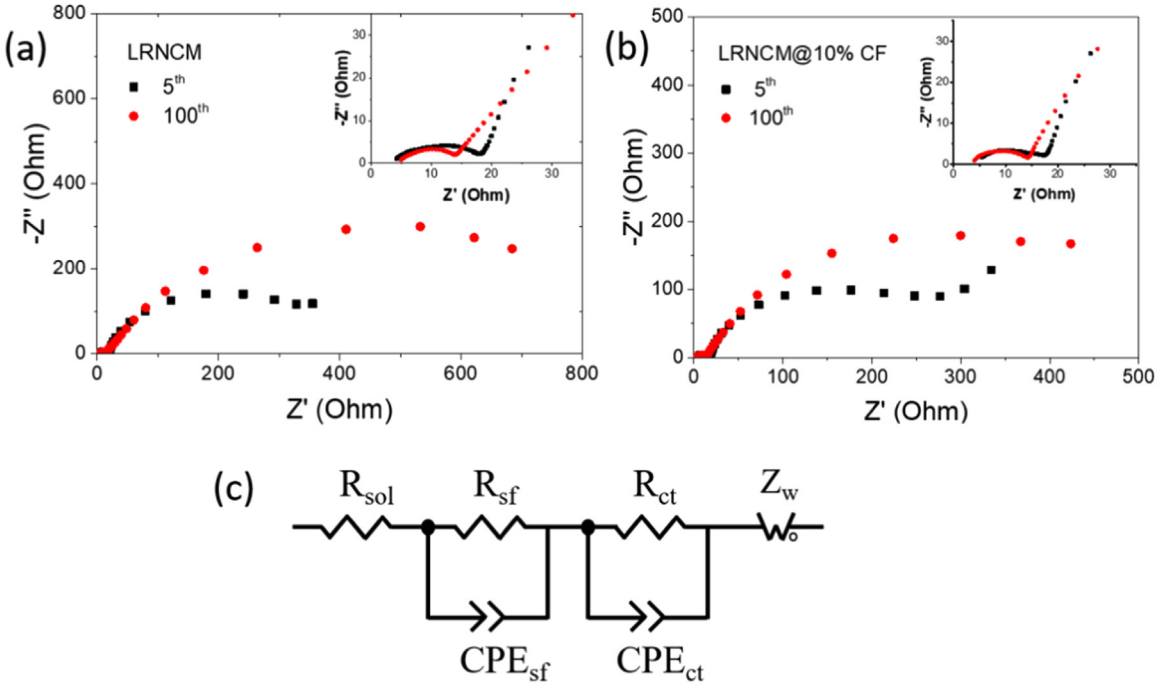

Fig. 7. EIS results of (a) pristine LRNCM and (b) LRNCM@10%CF; (c) equivalent circuit model.

Table 2
Impedance parameters of pristine LRNCM and LRNCM @10%CF charging to 4.8 V for 5th, 100th cycles.

Cycle number	LRNCM			LRNCM@10%CF		
	R_{sol} (Ω)	R_{sf} (Ω)	R_{ct} (Ω)	R_{sol} (Ω)	R_{sf} (Ω)	R_{ct} (Ω)
5th	3.1	16.1	330.1	2.8	17.3	250.3
100th	4.4	10.5	935.5	3.0	12.3	543.8

hand, after CF modification, the R_{sf} in fact increases from 16.1 Ω to 17.3 Ω after the 5th charging to 4.8 V, which is related to the presence of the LiF@carbon layer on the surface of LRNCM. On the other hand, R_{ct} decreases from 330.1 Ω to 250.3 Ω by 24% during the 5th charging to 4.8 V. With increasing cycle numbers, R_{ct} usually increase significantly due to the side reaction and structural degradation. After 100 cycles, the R_{ct} for LRNCM electrode is 935.5 Ω, whereas that of the LRNCM@10%CF electrode is only 543.8 Ω. Thus, the total resistance decreases from 946 to 556.2 Ω by 42% due to the CF modification. These results are ascribed to the coated LiF@carbon layer outside LRNCM which can inhibit the interfacial reactions between LRNCM and electrolyte and decrease the interfacial resistance. Therefore, after modification the interfacial stability of the LRNCM is significantly enhanced, resulting in the improvement of the rate capability and cycling performance.

4. Summary

In conclusion, the graphite fluoride-modified $Li_{1.14}Ni_{0.133}Co_{0.133}Mn_{0.544}O_2$ cathode materials are successfully prepared through a facile solvent evaporating process. On one hand, modification of graphite fluoride compensates the capacity loss during the first cycle to significantly improve initial coulombic efficiency. On the other hand, the reaction products form the LiF@carbon layer on the surface of the cathode, which decreases the interfacial reactions to improve the reversible capacity. After CF modification, the discharge capability is increased by 22% from 266 to 325 mAh g^{-1} at 0.1 C. The discharge capability at 1 C after 100 cycles is increased by 13% from 180 to 203 mAh g^{-1}. The EIS measurements prove that the LiF@carbon layer decreases cathode/electrolyte interfacial reactions, resulting in the decreases of the charge transfer resistance.

Acknowledgments

This work is supported partially by Beijing Natural Science Foundation (L172036), Joint Funds of the Equipment Pre-Research and Ministry of Education (6141A020225), Par-Eu Scholars Program, Science and Technology Beijing 100 Leading Talent Training Project, Beijing Municipal Science and Technology Project (Z161100002616039), the Fundamental Research Funds for the Central Universities (2016JQ01, 2017ZZD02) and the NCEPU "Double First-Class" Graduate Talent Cultivation Program.

Appendix A. Supplementary material

Supplementary data associated with this article can be found in the online version at doi:10.1016/j.ceramint.2018.09.147.

References

[1] H. Chen, Q. Hu, Z. Huang, Z. He, Z. Wang, H. Guo, X. Li, Synthesis and electrochemical study of Zr-doped $Li[Li_{0.2}Mn_{0.54}Ni_{0.13}Co_{0.13}]O_2$ as cathode material for Li-ion battery, Ceram. Int. 42 (2016) 263–269.
[2] X. Hu, H.J. Guo, J.X. Wang, Z.X. Wang, X.H. Li, Q.Y. Hu, W.J. Peng, Structural and electrochemical characterization of NH_4F-pretreated lithium-rich layered $Li[Li_{0.2}Ni_{0.13}Co_{0.13}Mn_{0.54}O]_2$ cathodes for lithium-ion batteries, Ceram. Int. 44 (2018) 14370–14376.
[3] S. Hy, H. Liu, M. Zhang, D. Qian, B.-J. Hwang, Y.S. Meng, Performance and design considerations for lithium excess layered oxide positive electrode materials for lithium ion batteries, Energy Environ. Sci. 9 (2016) 1931–1954.
[4] M.D. Radin, S. Hy, M. Sina, C. Fang, H. Liu, J. Vinckeviciute, M. Zhang, M.S. Whittingham, Y.S. Meng, A.Vd Ven, Narrowing the gap between theoretical and practical capacities in Li-ion layered oxide cathode materials, Adv. Energy Mater. 7 (2017) 1602888.
[5] H. Liu, Y. Chen, S. Hy, K. An, S. Venkatachalam, D. Qian, M. Zhang, Y.S. Meng, Operando lithium dynamics in the Li-rich layered oxide cathode material via neutron diffraction, Adv. Energy Mater. 6 (2016) 1502143.
[6] X. Li, Y. Feng, M. Li, W. Li, H. Wei, D. Song, Smart hybrids of Zn_2GeO_4 nanoparticles and ultrathin g-C_3N_4 layers: synergistic lithium storage and excellent electrochemical performance, Adv. Funct. Mater. 25 (2015) 6858–6866.
[7] J.W. Choi, D. Aurbach, Promise and reality of post-lithium-ion batteries with high

energy densities, Nat. Rev. Mater. 1 (2016) 16013.
[8] Y. Zhu, T. Yi, R. Zhu, A. Zhou, Increased cycling stability of $Li_4Ti_5O_{12}$-coated $LiMn_{1.5}Ni_{0.5}O_4$ as cathode material for lithium-ion batteries, Ceram. Int. 39 (2013) 3087–3094.
[9] J. Zhao, Z. Wang, H. Guo, X. Li, Z. He, T. Li, Synthesis and electrochemical characterization of Zn-doped Li-rich layered $Li[Li_{0.2}Mn_{0.54}Ni_{0.13}Co_{0.13}]O_2$ cathode material, Ceram. Int. 41 (2015) 11396–11401.
[10] Z. Xiao, J. Meng, Q. Li, X. Wang, M. Huang, Z. Liu, C. Han, L. Mai, Novel, MOF shell-derived surface modification of Li-rich layered oxide cathode for enhanced lithium storage, Sci. Bull. 63 (2018) 46–53.
[11] P.K. Nayak, E.M. Erickson, F. Schipper, T.R. Penki, N. Munichandraiah, P. Adelhelm, H. Sclar, F. Amalraj, B. Markovsky, D. Aurbach, Review on challenges and recent advances in the electrochemical performance of high capacity Li- and Mn-Rich cathode materials for Li-Ion batteries, Adv. Energy Mater. 8 (2018).
[12] H. Yu, H. Zhou, High-energy cathode materials (Li_2MnO_3-$LiMO_2$) for lithium-ion batteries, J. Phys. Chem. Lett. 4 (2013) 1268–1280.
[13] B. Strehle, K. Kleiner, R. Jung, F. Chesneau, M. Mendez, H.A. Gasteiger, M. Piana, The role of oxygen release from Li- and Mn-rich layered oxides during the first cycles investigated by on-line electrochemical mass spectrometry, J. Electrochem. Soc. 164 (2017) A400–A406.
[14] J. Huang, H. Liu, T. Hu, Y.S. Meng, J. Luo, Enhancing the electrochemical performance of Li-rich layered oxide Li1.13Ni0.3Mn0.57O2 via WO3 doping and accompanying spontaneous surface phase formation, J. Power Sources 375 (2018) 21–28.
[15] F. Wu, N. Li, Y. Su, H. Lu, L. Zhang, R. An, Z. Wang, L. Bao, S. Chen, Can surface modification be more effective to enhance the electrochemical performance of lithium rich materials? J. Mater. Chem. 22 (2012) 1489–1497.
[16] T. Zhao, L. Li, R. Chen, H. Wu, X. Zhang, S. Chen, M. Xie, F. Wu, J. Lu, K. Amine, Design of surface protective layer of LiF/FeF_3 nanoparticles in Li-rich cathode for high-capacity Li-ion batteries, Nano Energy 15 (2015) 164–176.
[17] H. Liu, D. Qian, M.G. Verde, M. Zhang, L. Baggetto, K. An, Y. Chen, K.J. Carroll, D. Lau, M. Chi, G.M. Veith, Y.S. Meng, Understanding the role of NH_4F and Al_2O_3 surface Co-modification on lithium-excess layered oxide $Li_{1.2}Ni_{0.2}Mn_{0.6}O_2$, ACS Appl. Mater. Interfaces 7 (2015) 19189–19200.
[18] B. Seteni, N. Rapulenyane, J.C. Ngila, S. Mpelane, H. Luo, Coating effect of $LiFePO_4$ and Al_2O_3 on $Li_{1.2}Mn_{0.54}Ni_{0.13}Co_{0.13}O_2$ cathode surface for lithium ion batteries, J. Power Sources 353 (2017) 210–220.
[19] H.D. Liu, J.J. Huang, D.N. Qian, S. Hy, C.C. Fang, J. Luo, Y.S. Meng, Communication-Enhancing the electrochemical performance of lithium-excess layered oxide $Li_{1.13}Ni_{0.3}Mn_{0.57}O_2$ via a facile nanoscale surface modification, J. Electrochem. Soc. 163 (2016) A971–A973.
[20] H. Zhuo, Y. Zhang, D. Wang, C. He, C. Zhu, Q. Zhang, C. Li, L. Sun, J. Liu, S. Chen, Insight into lithium-rich layered cathode materials $Li[Li_{0.1}Ni_{0.45}Mn_{0.45}]O_2$ in situ coated with graphene-like carbon, Electrochim. Acta 149 (2014) 42–48.
[21] M. Mar, Y. Ahmad, K. Guérin, M. Dubois, N. Batisse, Fluorinated exfoliated graphite as cathode materials for enhanced performances in primary lithium battery, Electrochim. Acta 227 (2017) 18–23.
[22] P.F. Fulvio, S.S. Brown, J. Adcock, R.T. Mayes, B. Guo, X.-G. Sun, S.M. Mahurin, G.M. Veith, S. Dai, Low-temperature fluorination of soft-templated mesoporous carbons for a high-power lithium/carbon fluoride battery, Chem. Mater. 23 (2011) 4420–4427.
[23] H. Yue, W. Zhang, H. Liu, Z. Liu, G. Zhong, Y. Yang, Synthesis and characterization of fluorinated carbon nanotubes for lithium primary batteries with high power density, Nanotechnology 24 (2013) 424003.
[24] M.G. Verde, H. Liu, K.J. Carroll, L. Baggetto, G.M. Veith, Y.S. Meng, Effect of morphology and manganese valence on the voltage fade and capacity retention of Li $[Li_{2/12}Ni_{3/12}Mn_{7/12}]O_2$, ACS Appl. Mater. Interfaces 6 (2014) 18868–18877.
[25] H. Liu, C.R. Fell, K. An, L. Cai, Y.S. Meng, In-situ neutron diffraction study of the $xLi_2MnO_3{\cdot}(1-x)LiMO_2$ (x = 0, 0.5; M = Ni, Mn, Co) layered oxide compounds during electrochemical cycling, J. Power Sources 240 (2013) 772–778.
[26] J. Xu, H.D. Liu, Y.S. Meng, Exploring Li substituted O3-structured layered oxides $NaLi_xNi_{1/3-x}Mn_{1/3+x}Co_{1/3-x}O_2$ (x = 0.07, 0.13, and 0.2) as promising cathode materials for rechargeable Na batteries, Electrochem. Commun. 60 (2015) 13–16.
[27] H.D. Liu, J. Xu, C.Z. Ma, Y.S. Meng, A new O3-type layered oxide cathode with high energy/power density for rechargeable Na batteries, Chem. Commun. 51 (2015) 4693–4696.
[28] H. Liu, H. Liu, S.H. Lapidus, Y.S. Meng, P.J. Chupas, K.W. Chapman, Sensitivity and limitations of structures from X-ray and neutron-based diffraction analyses of transition metal oxide lithium-battery electrodes, J. Electrochem. Soc. 164 (2017) A1802–A1811.
[29] H. Liu, H. Liu, I.D. Seymour, N. Chernova, K.M. Wiaderek, N.M. Trease, S. Hy, Y. Chen, K. An, M. Zhang, O.J. Borkiewicz, S.H. Lapidus, B. Qiu, Y. Xia, Z. Liu, P.J. Chupas, K.W. Chapman, M.S. Whittingham, C.P. Grey, Y.S. Meng, Identifying the chemical and structural irreversibility in $LiNi_{0.8}Co_{0.15}Al_{0.05}O_2$ – a model compound for classical layered intercalation, J. Mater. Chem. A 6 (2018) 4189–4198.
[30] Y. Kita, N. Watanabe, Y. Fujii, Chemical composition and crystal structure of graphite fluoride, J. Am. Chem. Soc. 101 (1979) 3832–3841.
[31] P. Meduri, H. Chen, J. Xiao, J.J. Martinez, T. Carlson, J.-G. Zhang, Z.D. Deng, Tunable electrochemical properties of fluorinated graphene, J. Mater. Chem. A 1 (2013) 7866.
[32] Y. Sato, K. Itoh, R. Hagiwara, T. Fukunaga, Y. Ito, On the so-called "semi-ionic" C–F bond character in fluorine–GIC, Carbon 42 (2004) 3243–3249.
[33] Y.K. Sun, S.T. Myung, B.C. Park, J. Prakash, I. Belharouak, K. Amine, High-energy cathode material for long-life and safe lithium batteries, Nat. Mater. 8 (2009) 320–324.
[34] T. Lei, Y. Li, Q. Su, G. Cao, W. Li, Y. Chen, L. Xue, S. Deng, High-voltage electrochemical performance of $LiNi_{0.5}Co_{0.2}Mn_{0.3}O_2$ cathode materials via Al concentration gradient modification, Ceram. Int. 44 (2018) 8809–8817.
[35] E. Rangasamy, J. Li, G. Sahu, N. Dudney, C. Liang, Pushing the theoretical limit of Li-CF_x batteries: a tale of bifunctional electrolyte, J. Am. Chem. Soc. 136 (2014) 6874–6877.
[36] P. Lam, R. Yazami, Physical characteristics and rate performance of $(CF_x)_n$ ($0.33 < x < 0.66$) in lithium batteries, J. Power Sources 153 (2006) 354–359.
[37] J. Huang, H. Liu, N. Zhou, K. An, Y.S. Meng, J. Luo, Enhancing the ion transport in $LiMn_{1.5}Ni_{0.5}O_4$ by altering the particle Wulff shape via anisotropic surface segregation, ACS Appl. Mater. Interfaces 9 (2017) 36745–36754.
[38] F. Ding, J. Li, F. Deng, G. Xu, Y. Liu, K. Yang, F. Kang, Surface heterostructure induced by $PrPO_4$ modification in $Li_{1.2}[Mn_{0.54}Ni_{0.13}Co_{0.13}]O_2$ cathode material for high-performance lithium-Ion batteries with mitigating voltage decay, ACS Appl. Mater. Interfaces 9 (2017) 27936–27945.
[39] Y.K. Sun, Z. Chen, H.J. Noh, D.J. Lee, H.G. Jung, Y. Ren, S. Wang, C.S. Yoon, S.T. Myung, K. Amine, Nanostructured high-energy cathode materials for advanced lithium batteries, Nat. Mater. 11 (2012) 942–947.
[40] X. Li, W. Li, M. Li, P. Cui, D. Chen, T. Gengenbach, L. Chu, H. Liu, G. Song, Glucose-assisted synthesis of the hierarchical TiO_2 nanowire@MoS_2 nanosheet nanocomposite and its synergistic lithium storage performance, J. Mater. Chem. A 3 (2015) 2762–2769.
[41] G. Wu, J. Chen, Y. Guo, X. Li, B. Luo, L. Chu, Y. Han, B. Jiang, L. Xu, M. Li, Freestanding sodium-ion batteries electrode using graphene foam coaxially integrated with TiO_2 nanosheets, J. Electrochem. Soc. 164 (2017) A3060–A3067.
[42] X.Y. Qiu, Q.C. Zhuang, Q.Q. Zhang, R. Cao, Y.H. Qiang, P.Z. Ying, S.G. Sun, Investigation of layered $LiNi_{1/3}Co_{1/3}Mn_{1/3}O_2$ cathode of lithium ion battery by electrochemical impedance spectroscopy, J. Electroanal. Chem. 687 (2012) 35–44.
[43] L. Chu, M. Li, X. Li, Y. Wang, Z. Wan, S. Dou, D. Song, Y. Li, B. Jiang, High performance NiO microsphere anode assembled from porous nanosheets for lithium-ion batteries, RSC Adv. 5 (2015) 49765–49770.
[44] X. Li, G. Wu, X. Liu, W. Li, M. Li, Orderly integration of porous TiO_2(B) nanosheets into bunchy hierarchical structure for high-rate and ultralong-lifespan lithium-ion batteries, Nano Energy 31 (2017) 1–8.